NO

Technical Report No. 32-654

Comparisons of Experimental with Predicted Wall Static-Pressure Distributions in Conical Supersonic Nozzles

L. H. Back
P. F. Massier
H. L. Gier

JET PROPULSION LABORATORY
CALIFORNIA INSTITUTE OF TECHNOLOGY
PASADENA, CALIFORNIA

October 15, 1964

Technical Report No. 32-654

Comparisons of Experimental with Predicted Wall Static-Pressure Distributions in Conical Supersonic Nozzles

L. H. Back
P. F. Massier
H. L. Gier

D. R. Bartz, Chief
Propulsion Research Section

JET PROPULSION LABORATORY
CALIFORNIA INSTITUTE OF TECHNOLOGY
PASADENA, CALIFORNIA

October 15, 1964

Prepared Under Contract No. NAS 7-100
National Aeronautics & Space Administration

CONTENTS

I. Introduction 1

II. Instrumentation 2

III. Static-Pressure Distributions 6

IV. Two-Dimensional Flow Predictions 8

V. Static-Pressure Tap Size 9

VI. Separation Pressures 11

VII. Mass Flow Rate 12

VIII. Thrust Ratios 13

IX. Sonic Line 14

X. Mass Flux Ratios 14

XI. Conclusions 15

Nomenclature 16

References 16

Table 1. Comparison of predicted and experimental sonic line intersection with edge of boundary layer at $T_t = 1500°R$ (cooled walls) 14

FIGURES

1. Flow and instrumentation diagram 2

2. Static-to-stagnation pressure ratios along the 30–15-deg nozzle . . . 3

3. Static-to-stagnation pressure ratios with various nozzle-inlet configurations 4

4. Static-to-stagnation pressure ratios along the 45–15-deg nozzle . . . 5

5. Measured to one-dimensional static-pressure ratios along the nozzles (One-dimensional flow predictions are for $\gamma = 1.40$ and measured values are the averages of the hot-flow cooled-wall values shown in Fig. 2 [A] and Fig. 4.) 7

6. Static-to-stagnation pressure ratios along the 2.51–1 nozzle with different size pressure taps 10

7. Separation to ambient-pressure ratios for various nozzles 11

FIGURES (Cont'd)

8. Flow coefficients 12

9. Variation of thrust ratio with expansion-area ratio (Curves were obtained from averaged p/p_1 ratios shown in Fig. 5.) 13

10. Local to one-dimensional mass flux ratios along the nozzles (Values were determined from averaged p/p_1 ratios shown in Fig. 5.) 14

ABSTRACT

Wall static pressures have been measured at stagnation pressures between 45 and 250 psia in circular-arc-throat conical nozzles with half-angles of convergence of 30 and 45 deg, 15-deg half-angles of divergence, and expansion-area ratios to 6.6. In several additional nozzles, the convergent section was formed by circular arcs. The ratios of throat radius of curvature to throat radius, r_c/r_{th}, were 2.0 and 0.625. These measurements, made with air either at a stagnation temperature of 530°R or heated by the combustion of methanol to 1500°R, indicate considerable deviations from one-dimensional isentropic flow predictions in the throat region. For one nozzle, these amount to as much as 45%. Deviations of a smaller magnitude are also found in the conical sections. The static-pressure measurements for underexpanded operation were insensitive both to the effects of cooled and uncooled walls and to variations in nozzle-inlet boundary-layer thicknesses. Static-pressure measurements in the throat and divergent regions of nozzles with the same r_c/r_{th} and half-angle of divergence were found to be independent of the various inlet configurations. Differences up to 7% in static-pressure tap readings were found between tap sizes of 0.010- and 0.040-in. diameter, with the smaller tap reading the lower pressure. Some separation pressure data are also presented for overexpanded nozzle operation; these indicate that the separation point moves downstream with wall cooling for tests at the same stagnation pressure. Other flow features presented in terms of deviations from one-dimensional flow include flow coefficients, thrust ratios, and local mass fluxes at the edge of the boundary layer. Also, the location of the sonic line at the edge of the boundary layer was deduced from the wall static-pressure measurements. Two-dimensional flow predictions are in close agreement in the throat region with the data for the nozzles with $r_c/r_{th} = 2.0$ but inadequate for the one with $r_c/r_{th} = 0.625$.

I. INTRODUCTION

In accelerating gas flows to supersonic velocities through conical nozzles, there can be appreciable deviations from one-dimensional flow, as indicated by measured wall static-pressure distributions. These deviations, which result from radial velocity components caused by the taper and curvature of the nozzle, are noted in Ref. 1. Similar deviations are observed in Refs. 2, 3, 4, and 5, in which measurements were made in the divergent region of conical nozzles, and in Ref. 6, where a few measurements were made in the conical convergent region. In Ref. 7, local velocity measurements in the throat region indicated the two-dimensionality of the flow.

In this discussion, measured wall static-pressure distributions are presented for conical nozzles to show the dependence of the deviations from one-dimensional isentropic flow on nozzle configuration and the region over which these deviations extend. The conical nozzles investigated have 30- and 45-deg half-angles of convergence, 15-deg half-angles of divergence, circular-arc entrance and throat sections, and expansion-area ratios up to 6.6. The ratios of throat radius of curvature to throat radius were 2.0 and 0.625. The effect of inlet configuration was investigated in other nozzles with the convergent sections formed by circular arcs.

Operating conditions spanned stagnation pressures from 45 to 250 psia and stagnation temperatures from 530 to 2000°R, with data reported at 530 and 1500°R. The ambient pressure was atmospheric. At the lower stagnation temperature of 530°R, compressed air was used and the nozzles were uncooled. The higher stagnation temperatures were obtained by heating compressed air by the combustion of methanol. The products of combustion were then mixed to obtain uniformity before entering the nozzles, and at these higher temperatures, the nozzle walls were cooled. At the highest stagnation temperature, the total heat transfer from the gas to the nozzle wall was less than 1% of the total energy of the gas at the nozzle inlet so that the flow was nearly adiabatic in all cases. The products of combustion could be treated approximately as air, since the methanol-to-air mass flow-rate ratio was small.

Boundary-layer thicknesses at the nozzle inlet were varied from about 5 to 45% of the inlet radius to investigate boundary-layer displacement effects. The effect of wall static-pressure tap size on the readings was also investigated. At the lower stagnation pressures, the nozzles were overexpanded, and the associated separation pressures are presented both for hot-flow cooled-wall and cold-flow operation. Other features of the flow are included in terms of deviations from one-dimensional isentropic flow. For over-all nozzle performance, flow coefficients and thrust ratios are shown. Local deviations in the mass flux at the edge of the boundary layer calculated from the measured wall static pressures are included, as is the sonic line location.

Analytical two-dimensional flow predictions are compared to the data to indicate the extent to which the flow is predictable.

II. INSTRUMENTATION

Figure 1 is the flow and instrumentation diagram of the system to which the nozzles were attached. Stagnation pressure was measured just upstream of the approach section, the length of which could be adjusted to specified values. Changes in length were made to vary the nozzle-inlet boundary-layer thickness. These turbulent boundary-layer thicknesses were estimated from measurements described in Ref. 1. The approach section was cooled at the higher stagnation temperature of 1500°R. Stagnation temperature was determined by averaging the readings of two shielded thermocouples placed 0.25 in. upstream of the nozzle inlet. These two thermocouples, located 1 in. from the centerline, were spaced 180 deg apart circumferentially and generally read within 2% of each other. The air mass flow rate was measured with an orifice, and for the hot-flow tests, a rotometer was used to measure the mass flow rate of methanol. The accuracy of the total mass flow rate is estimated to be 1% at stagnation pressures above about 100 psia. At lower stagnation pressures, the readings are less accurate.

For the 30–15- and 45–15-deg nozzles shown in Figs. 2 and 4, the wall static-pressure taps were 0.040- and 0.020-in. diameter, respectively. The hole depth-to-diameter ratio was about 8 for the 30–15-deg nozzle and essentially infinity for the 45–15-deg nozzle. For the nozzles shown in Fig. 3, the tap diameter was 0.020 in. and the hole depth-to-diameter ratio was 4. These holes were as sharp-edged as they could be made by drilling and then smoothing the burrs with emery cloth. The axial location of each tap was known to 0.002 in., and the taps were spaced circumferentially and axially along each nozzle wall. The static pressures were measured either with mercury manometers or, at the higher pressures, with Heise gages which had 0.25-psia marked increments. The accuracy of the readings is dictated by the difference between the static and stagnation pressures and thus depends on location in the nozzle and on the stagnation pressure. The largest estimated error would be in the nozzle-inlet region at the lowest stagnation pressures, where an error between the actual static and stagnation pressures could have amounted to about 5%. However, in terms of the static-to-stagnation pressure ratio p/p_t, the error would be less than 0.1%. This error would be smaller yet through the throat and divergent regions, as well as at higher stagnation pressures. Considerably larger differences are found with different size taps, as discussed in Section V.

For hot-flow cooled-wall operation, wall temperatures were determined from thermocouples embedded in the wall of the 30–15-deg nozzle and from calorimetric wall heat-flux measurements with the 45–15-deg nozzle.

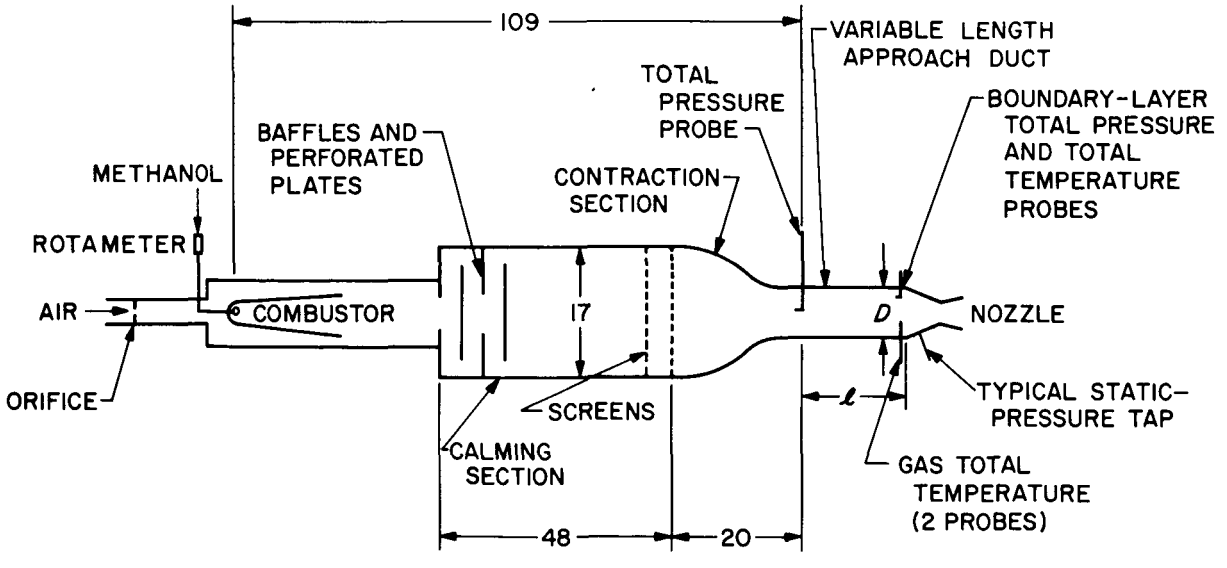

Fig. 1. Flow and instrumentation diagram

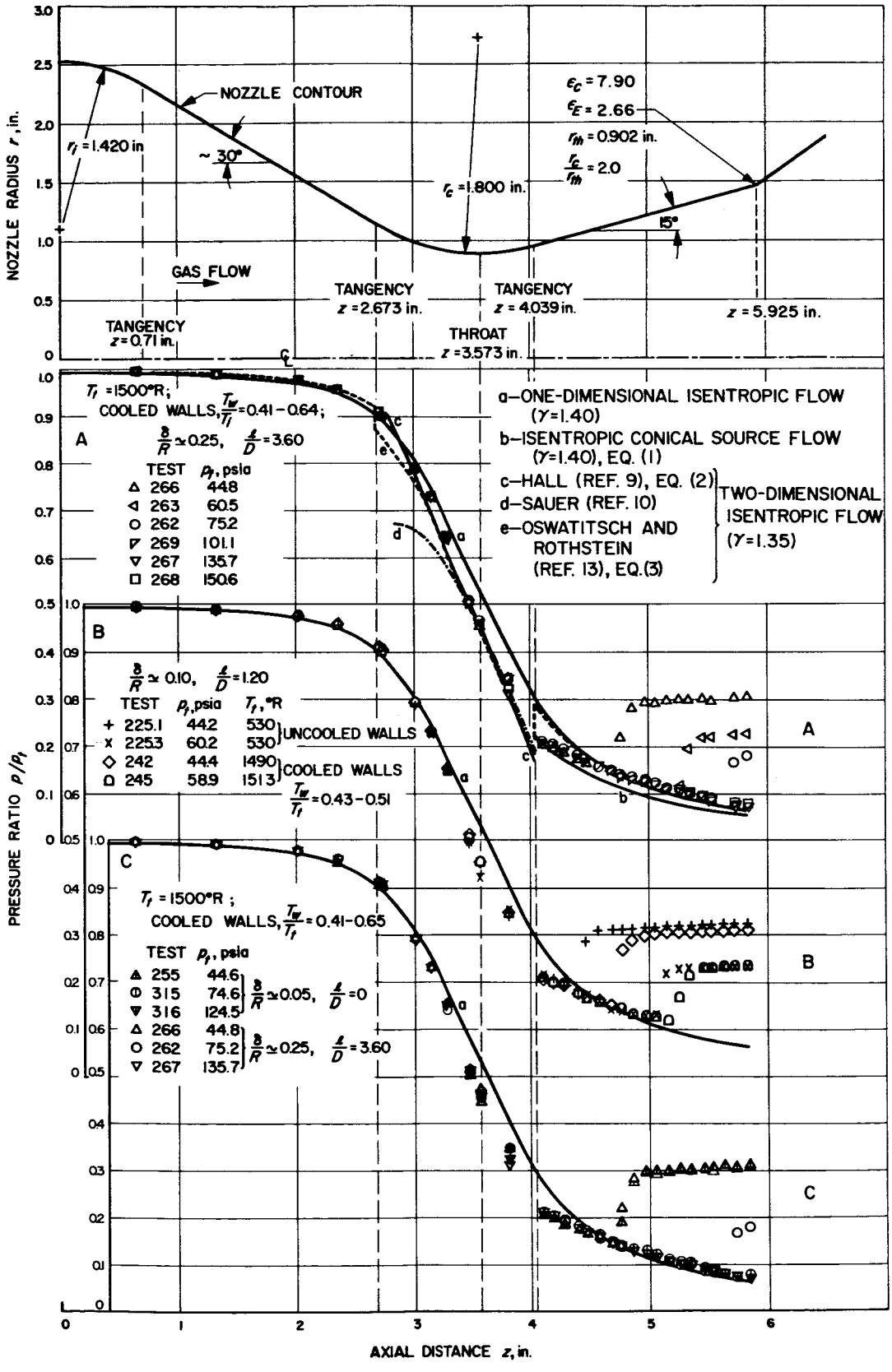

Fig. 2. Static-to-stagnation pressure ratios along the 30–15-deg nozzle

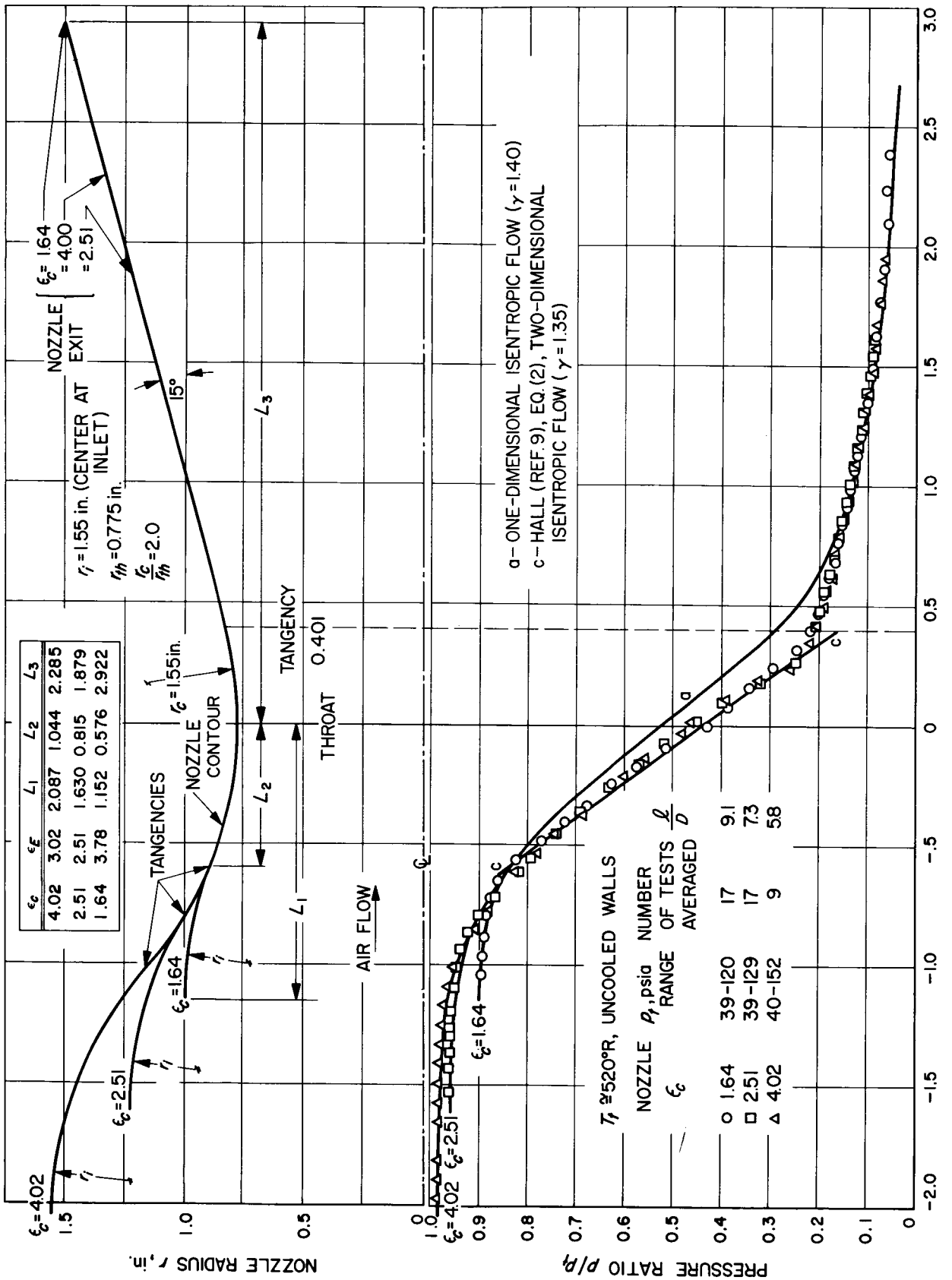

Fig. 3. Static-to-stagnation pressure ratios with various nozzle-inlet configurations

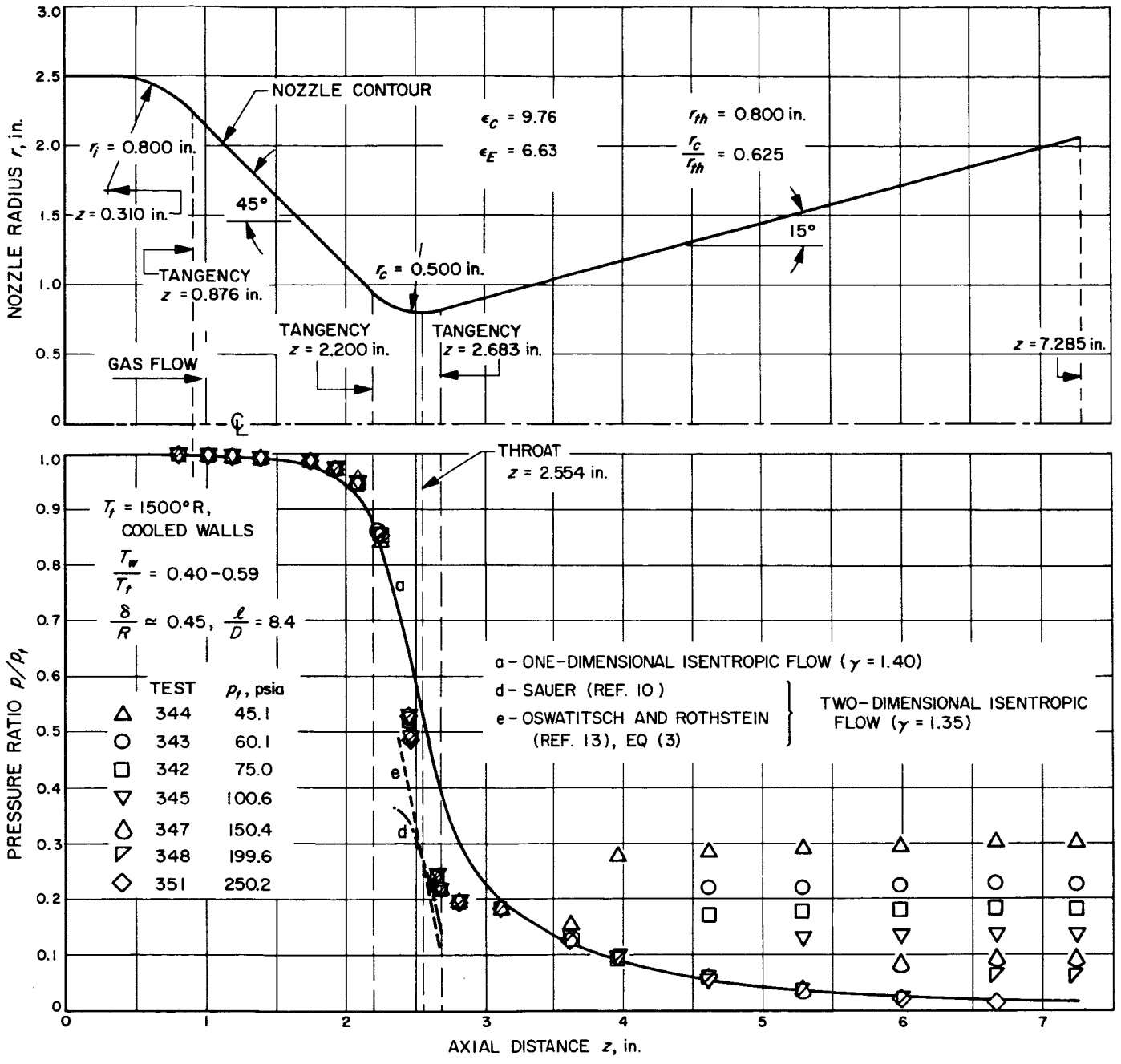

Fig. 4. Static-to-stagnation pressure ratios along the 45–15-deg nozzle

III. STATIC-PRESSURE DISTRIBUTIONS

Measured static-to-stagnation pressure ratios are shown in Fig. 2A for the 30–15-deg nozzle over a range of stagnation pressures from 45 to 150 psia at a stagnation temperature of 1500°R, with cooled walls. The upper limit of 150 psia was dictated by manometer limitations at the time the tests were made. From boundary-layer traverses, the ratio of inlet boundary-layer thickness to nozzle-inlet radius was estimated at about $\delta/R \simeq 0.25$. The pressure ratios are nearly invariant with stagnation pressure except in the flow-separation region, where the rise in static pressure is caused by overexpanded nozzle operation. In the throat region, there is some data spread, but it does not appear to vary systematically with stagnation pressure. Considerable deviations from the one-dimensional isentropic flow prediction ($\gamma = 1.40$), shown as curve "a," are apparent in the circular-arc-throat region; in particular, the measured pressures are as much as about 30% below the prediction just downstream of the throat. Deviations of a smaller magnitude are observable in the inlet and conical convergent section, where the data are slightly above the one-dimensional flow prediction. Near the tangency of the circular-arc throat and conical divergent section, the measured pressure ratios change slope abruptly and cross over the one-dimensional flow prediction further downstream. A one-dimensional isentropic flow prediction with variable specific heat was also made and found to be at most 2% above the prediction shown for $\gamma = 1.40$. This small difference indicated the prediction with $\gamma = 1.40$ to be adequate for comparison purposes if the entire nozzle flow region is considered.*

Another one-dimensional flow prediction referred to in the literature is that for conical source flow in the divergent region. The predicted wall static-pressure distribution for isentropic flow ($\gamma = \text{const.}$) is

$$\frac{p}{p_b} = \left\{1 - \frac{\gamma - 1}{2} M_b^2 \left[\frac{\left(\frac{s_b}{s}\right)^4}{\left(\frac{p}{p_b}\right)^{2/\gamma}} - 1\right]\right\}^{\gamma/(\gamma-1)} \qquad (1)$$

The subscript b denotes a point along the conical wall where the indicated variables are known, and s is the radial distance from the source. If the experimental pressure and corresponding Mach number at the circular-arc-throat conical tangency point are used, Eq. (1) is shown in Fig. 2A by curve "b" to predict substantially lower static pressures in the conical section than those obtained experimentally. Although better agreement could be obtained if the prediction were initiated downstream of the tangency, the comparison nevertheless indicates that the actual flow differs from conical source flow in the first part of the conical section.

Figure 2B shows hot-flow cooled-wall tests and cold-flow tests with a shorter approach length ($l/D = 1.2$), such that $\delta/R \simeq 0.10$. The effect of wall cooling is seen to alter the measured pressure ratios negligibly except in the flow separation region, where, at the same stagnation pressure, the separation point has moved downstream with wall cooling. Since, even with wall cooling, the flow is nearly adiabatic, as was mentioned in the Introduction, the effect of wall cooling would be to alter the nozzle flow cross-sectional area as a result of the boundary-layer displacement effect. The effect of γ would be small, as noted previously. Cooled walls tend to decrease δ^* below uncooled-wall values, and if the wall cooling is large enough, δ^* can become negative. However, predicted values of δ^* from the turbulent boundary-layer analysis of Ref. 8 were small compared to the nozzle radius, so that the displacement-effect correction was negligible. To illustrate the correction in the nozzle-inlet region in which δ^* is largest, for test 262, where $\delta^*/r = 0.020$, the predicted pressure ratio p/p_t was about 0.6% below the one-dimensional flow prediction, whereas the data are slightly above. Predicted values of δ^* become negative upstream of the throat, and for the same test, $\delta^*/r = -0.0041$ just downstream of the throat, with the predicted pressure ratio p/p_t being only about 0.1% below the one-dimensional flow prediction.

In Fig. 2C, hot-flow cooled-wall tests are shown for inlet boundary-layer thicknesses $\delta/R \simeq 0.05$ and 0.25, which correspond to $l/D = 0$ and 3.6, respectively. The effect on the measured pressure ratio is not discernible because of the large flow acceleration, which, in the convergent region, rapidly diminishes the boundary-layer thickness as well as the displacement thickness. Similarly to the effect of wall cooling, the predicted displacement-thickness correction was found to alter the predicted pressure ratio negligibly.

To investigate the effect of inlet configuration, measured pressure ratios are shown in Fig. 3 for nozzles of different contraction-area ratios but having the same

*For subsequent comparisons in the throat region, γ differs little from the stagnation condition value of 1.35 used.

throat radius, throat radius of curvature, and half-angle of divergence. The convergent sections were formed by circular arcs of equal radii of curvature. For comparison purposes, the cold-flow data shown are average values for each nozzle over the range of stagnation pressures indicated in the Figure. Separated flow data (not shown in the Figure) are discussed in Section VI. Through the throat and divergent regions, the measured pressure ratios are essentially independent of inlet configuration and depend only on the local nozzle contour. The magnitudes of the deviations from one-dimensional isentropic flow (curve "a") are similar to those found with the 30–15-deg nozzle (Fig. 2), which has the same ratio of throat radius of curvature to throat radius ($r_c/r_{th} = 2.0$) and half-angle of divergence as the nozzles shown in Fig. 3.

The effect of throat configuration is shown by comparing Fig. 4 to Fig. 2. In Fig. 4, measured pressure ratios for the 45–15-deg nozzle are shown for a stagnation-pressure range from 45 to 250 psia and a stagnation temperature of 1500°R. Because of the smaller throat radius of curvature to throat radius of 0.625, compared to 2.0 for the 30–15-deg nozzle, there are larger deviations from the one-dimensional isentropic-flow pressure ratio in the throat region. These amount to as much as 45% just downstream of the throat. In the conical convergent section, there are also larger deviations from one-dimensional flow than with the 30–15-deg nozzle because of the larger 45-deg half-angle of convergence. In addition, at the higher expansion-area ratios of the 45–15-deg nozzle, the data once more cross over and become less than the one-dimensional flow prediction. With the 45–15-deg nozzle, only hot-flow cooled-wall data were obtained, and a larger upstream length ($l/D = 8.4$) was used such that $\delta/R \simeq 0.45$. Although no data were obtained with a thinner inlet boundary-layer thickness, the measured pressure ratios are expected to be altered negligibly based on both experimental observations with the 30–15-deg nozzle and theoretical predictions.

To compare the magnitude of the deviations from one-dimensional flow and the region over which they extend, the ratio p/p_1 is shown in Fig. 5 as a function of the area ratios for the 30–15- and 45–15-deg nozzles. The measured pressures shown are from the average of the hot-flow cooled-wall ratios p/p_t, shown in Figs. 2A and 4 over the stagnation pressure ranges indicated. No separation flow data are shown. Worthy of note is the rather sharp dip in p/p_1 just downstream of the throat to its minimum value. For the 30–15-deg nozzle, the minimum value is not well defined; however, for the nozzles shown in Fig. 3, which have the same values of r_c/r_{th} and half-angle of divergence as the 30–15-deg nozzle, the minimum value is about 0.70. Actually, the deviations from one-dimensional flow are probably larger than those indicated where $p/p_1 < 1$, since a smaller pressure tap would read a lower value, which is believed to be nearer the true static pressure. The effect of static-pressure tap size is discussed in Section V.

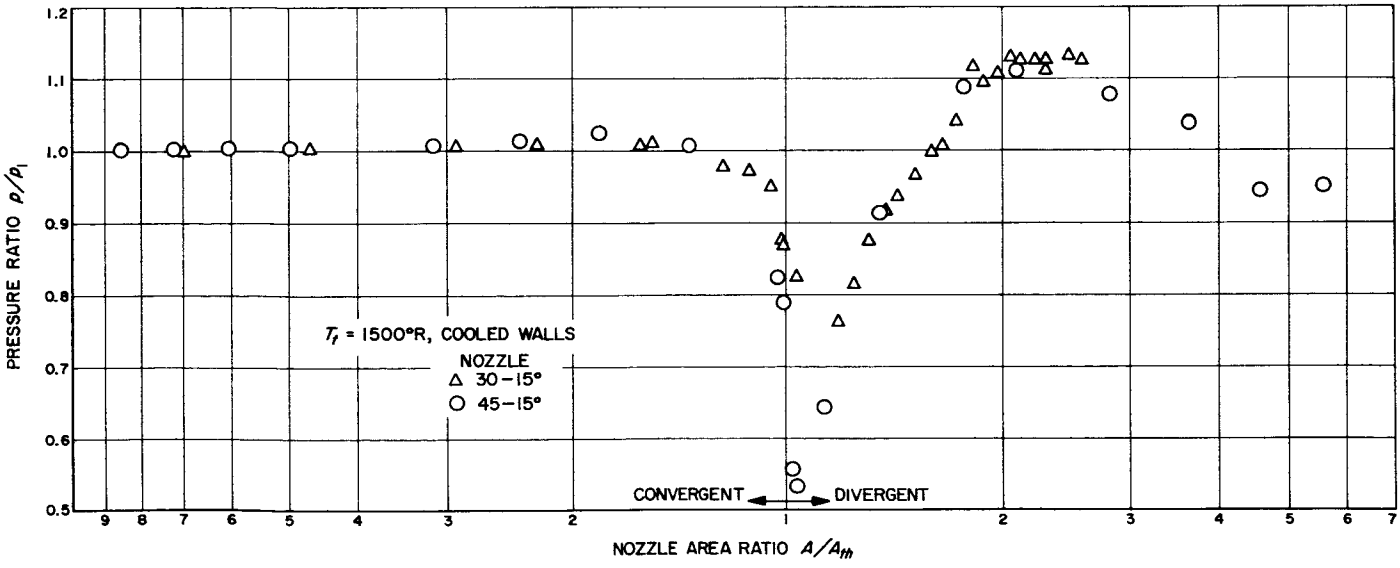

Fig. 5. Measured to one-dimensional static-pressure ratios along the nozzles (One-dimensional flow predictions are for $\gamma = 1.40$ and measured values are the averages of the hot-flow cooled-wall values shown in Fig. 2 [A] and Fig. 4.)

IV. TWO-DIMENSIONAL FLOW PREDICTIONS

Exact solutions of the two-dimensional isentropic-flow equations are virtually nonexistent for flow regimes throughout a supersonic nozzle. Approximate solutions consist either of calculating the flow field by numerical or graphical techniques or of obtaining analytical solutions in particular flow regions. Since deviations from one-dimensional flow are largest near the throat, this region is of primary concern. Also, a solution in this region is needed to initiate the method-of-characteristics solution in the supersonic region.

In the throat region, Hall (Ref. 9) obtained a solution for the velocity field for isentropic, irrotational flow (γ = const.) by a series expansion of the velocity components in inverse powers of r_c/r_{th}. The first three terms for the velocity components in the series solution were calculated and appear in the reference. From these, the wall static-to-stagnation pressure ratio can be calculated:

$$\frac{p}{p_t} = \left[1 - \frac{\gamma - 1}{\gamma + 1}\overline{V}^2\right]^{\gamma/(\gamma-1)} \tag{2}$$

where $\overline{V}$ is the local velocity V at the wall, nondimensionalized with respect to the speed of sound at the sonic condition a*. The prediction from Eq. (2) is shown in Fig. 2A by curve "c," which agrees well with the measured pressure distributions in the throat vicinity. In the regions which extend to the circular-arc-throat conical tangencies, the requirement that the velocity at the wall be parallel to the wall is not exactly satisfied as a consequence of the solution method; this undoubtedly leads to the inferior prediction near these tangencies.

The correspondence of the prediction from Eq. (2) with the data is equally good for the nozzles with various inlet configurations, as shown in Fig. 3 by curve "c." It should be noted that Hall's prediction depends only on throat configuration through the ratio r_c/r_{th} and not on inlet configuration. The measured pressure ratios in the throat region shown in Fig. 3 display this same trend.

For the 45–15-deg nozzle ($r_c/r_{th} = 0.625$), the prediction is not applicable since the series solution diverges for $r_c/r_{th} < 1$. Instead, Fig. 4 shows as curve "d" the Sauer prediction (Ref. 10), which, as Hall has pointed out, is the first-term approximation in his series solution. This prediction is considerably below the data for the 45–15-deg nozzle. In Fig. 2A (curve "d"), this prediction indicates the improvement upstream of the throat afforded by the Hall solution, curve "c," in which three terms are used. However, at and downstream of the throat, there is little difference between the first and third approximations.

It would be of interest to compare to the data predictions from the irrotational method of characteristics in the supersonic region; however, flow conditions in circular-arc-throat conical nozzles predicted by Darwell and Badham (Ref. 11) and Migdal and Landis (Ref. 12) are such as to invalidate the prediction method. Both of these analyses reveal predicted flow conditions near the nozzle axis which would lead to shock formation. This occurs where Mach lines originating just downstream of the circular-arc-throat conical tangency meet the nozzle axis. Darwell and Badham discuss the prediction in detail with respect to the accuracy of the numerical solution and its initiation, using either Hall's throat solution (Ref. 9) or Sauer's solution (Ref. 10). As indicated in Fig. 2A, for the 30–15-deg nozzle with $r_c/r_{th} = 2.0$, either of these solutions should provide a good approximation to the actual flow in the region of interest. It should be noted that boundary-layer displacement effects, not accounted for in these predictions, do influence the nozzle free-stream flow boundary to some extent, which can alter the predicted flow field. Whether or not shock formation actually occurs along the nozzle axis can only be decided by experimental observation. Rather than wall static-pressure measurements, either total pressure-probe traverses along the axis of conical nozzles or some means of visual observation in a transparent nozzle with a sufficiently long divergence section would be required.

Another approximate solution valid throughout the nozzle, providing that wall curvature effects are not large, is the prediction by Oswatitsch and Rothstein (Ref. 13):

$$\frac{p}{p_t} = \left[1 - \frac{\gamma - 1}{2}\left(M_1 \frac{a_1}{a_t}\right)^2 \left(\frac{V}{u_1}\right)^2\right]^{\gamma/(\gamma-1)} \tag{3}$$

where

$$\frac{V}{u_1} = \left[\left\{1 + \frac{1}{2}\left[\frac{r}{2}\frac{d^2r}{dz^2} + \frac{1}{4}\frac{\frac{du_1}{dz}}{u_1} r \frac{dr}{dz} - \left(\frac{dr}{dz}\right)^2\right]\right\}^2 + \left(\frac{dr}{dz}\right)^2\right]^{1/2}$$

The subscript 1 denotes average quantities for one-dimensional isentropic flow, in which $\gamma = \text{const}$. For calculation purposes, it is convenient to use the relation

$$\frac{1}{u_1}\frac{du_1}{dz} = \frac{2}{r}\frac{\frac{dr}{dz}}{(M_1^2 - 1)}$$

In the prediction which applies for a constant γ, the velocity distribution is computed from the local configuration of the wall. The requirement that the fluid velocity at the wall be parallel to the wall is not exactly satisfied because of the way in which the solution was obtained. The prediction from Eq. (3) is shown in Fig. 2A as curve "e" to be in close agreement with the Hall prediction and, thus, the data in the throat vicinity of the 30–15-deg nozzle. At the circular-arc-throat conical tangencies the prediction is discontinuous because of d^2r/dz^2; these discontinuities are indicated by vertical dashed lines. Near the tangencies, the solution becomes more approximate, since the restrictions on the magnitude of the nozzle radius and its derivatives implied in the analysis are not satisfied.

The 45–15-deg nozzle contour deviates even further from the restrictions imposed by this analysis; however, for comparison, this prediction is shown in Fig. 4 as curve "e" in a narrow part of the throat region. The rather sharp decrease in static pressure is predicted, but the prediction is below the data.

V. STATIC-PRESSURE TAP SIZE

The presence of a static-pressure hole causes some flow disturbance which alters the measured static pressure from the true value. For sharp-edged holes, deeper than about 2 diameters, measured static pressures in flows with negligible pressure gradients have been found to increase with hole size; it is believed that the small holes read nearer the true static pressure. Other effects, such as slight burrs and the presence of foreign particles, have been found to alter the readings as well. For nozzle flow, in addition to the pressure gradient induced in the flow by the presence of the hole, the external pressure gradient is superimposed in the flow direction. The flow disturbance is thus expected to increase with hole size because a larger pressure drop exists across the hole than when the free-stream flow is not accelerating.

To investigate the effect of hole size on the static-pressure readings, the 2.51–1 nozzle shown in Fig. 3 was instrumented with 0.010- and 0.040-in.-diameter tap pairs. As mentioned before, the holes were as sharp-edged as they could be made by smoothing with emery cloth any surface burrs that were produced by drilling. The hole depth-to-diameter ratio was about 3. Static-pressure distributions were obtained over a range of stagnation pressures from 45 to 170 psia, with air at a stagnation temperature of 520°R (uncooled walls). Two of these distributions are shown in Fig. 6. To allow a direct comparison of the differences in the readings, the lower part of Fig. 6 also shows the percentage difference between the 0.010- and 0.040-in.-diameter tap readings at locations where these two taps were axially within 0.002 in. of each other. This is the limit to which the axial location of the taps is known. As indicated by comparison of the smallest and largest tap readings at the same axial location, the smallest tap has the lower reading, as has been observed in flows with negligible acceleration. The percentage difference in the tap readings increases from about 0.1% in the nozzle-inlet region as the free-stream velocity increases. In the throat region, where the pressure gradient is largest, the differences spread considerably, with a value as large as 7% indicated for the high stagnation-pressure test. In the divergent region, the difference remains relatively constant at about 3% for this test. For the low stagnation-pressure test, the maximum difference of about 4% diminishes in the divergent region and, in the flow separation region, is hardly discernible as a result of relatively low reverse flow velocities.

The trends of the differences shown for the two tests were typical of those found at intermediate stagnation

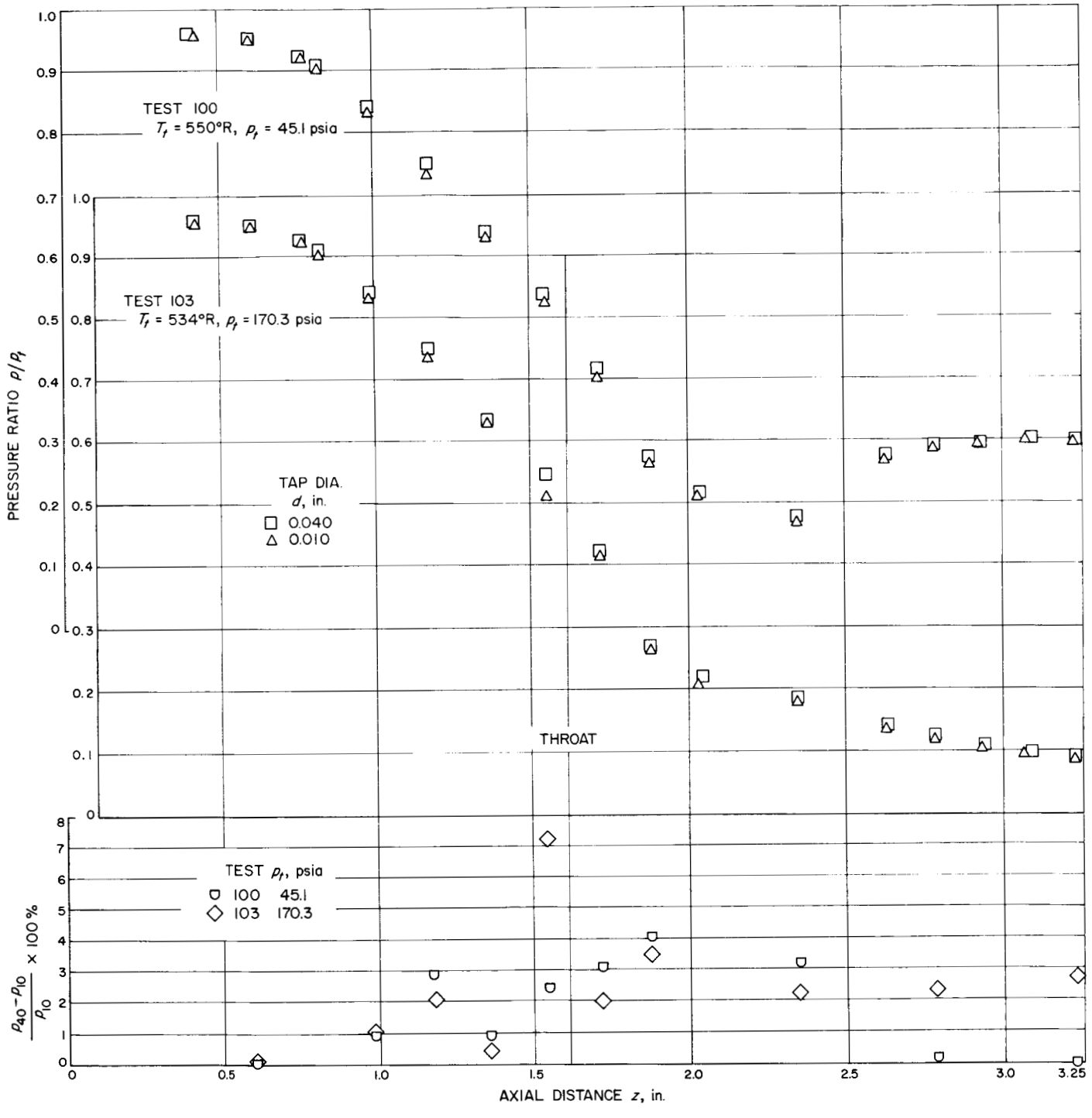

Fig. 6. Static-to-stagnation pressure ratios along the 2.51–1 nozzle with different size pressure taps

pressures of 75, 100, and 125 psia, and duplicate tests at some of the pressures indicated the data to be reproducible. The 0.002-in. uncertainty in the axial distance between the 0.010- and 0.040-in.-diameter tap pairs would alter the percentage differences shown in Fig. 6 by 0.1 at most. In a system in which pressure gradients can exceed those along the 2.51–1 nozzle, Jaivin (Ref. 14) found differences of the same magnitude as those shown in Fig. 6 for tap diameters ranging from 0.0016 to 0.019 in. by measuring the pressure distributions along a flat plate on which a liquid jet impinged. In that investigation, a limiting value of the tap size was found for which no

further change in the measured pressure distribution was observed; a 0.004-in.-diameter tap read the same as the 0.0016-in.-diameter tap.

To indicate the magnitude of the differences between the tap readings in another way, reference is made to an estimate of the static-pressure tap error. By dimensional analysis for a low-speed, essentially constant-property turbulent boundary layer with negligible flow acceleration, Livesey et al. (Ref. 15) and others give the error Δp for deep holes:

$$\frac{\Delta p}{\tau} = \frac{\Delta p}{\tau}(d^*)$$

where $d^* = d(\tau/\rho)^{1/2}/\nu$, d is the tap diameter, and τ is the wall shear stress. According to experimental measurements by Livesey et al. and others, $\Delta p/\tau$ increases monotonically with d^* to about 3 at $d^* \cong 900$, the limit at which measurements have been made. By comparison, in the throat region for the highest stagnation-pressure test, values of $(p_{40} - p_{10})/\tau$ are as large as 40; the corresponding value of d^* based on the 0.040-in.-diameter tap is about 6200. For the lowest stagnation-pressure test, the predicted value in the throat region is less, $(p_{40} - p_{10})/\tau \cong 10$, as is the corresponding value $d^* \cong 1900$. In these estimates, the wall shear stress was predicted from the turbulent boundary-layer analysis of Ref. 8.

Unfortunately, since the true static pressure is not known, one can only conclude from the data shown in Fig. 6 that the static-pressure distributions shown in Figs. 2, 3, and 4 are probably slightly higher than the true ones, with the deviations from one-dimensional flow, particularly in the throat region, exceeding those shown.

VI. SEPARATION PRESSURES

For overexpanded nozzle operation, the ratios of separation to ambient pressure are shown in Fig. 7 for nozzles that have $r_c/r_{th} = 2.0$. There were too few pressure taps in the divergent region of the 45–15-deg nozzle for a meaningful representation. The data are shown by the barred vertical lines. The upper bar is the tap reading upstream of the separation point; the lower bar would be that at the succeeding tap if separation had not occurred and was determined from higher stagnation-pressure tests. Thus, the actual value lies between the values shown. The Mach number at separation was calculated for isentropic flow ($\gamma = 1.4$) based on the average separation pressure. The hot-flow cooled-wall separation-to-ambient pressure ratios (shaded symbols) are generally about 5 to 10% below the cold-flow values (open symbols). These lower values correspond to a relocation of the separation point downstream with wall cooling, as was observed in Fig. 2B by comparing the hot-flow cooled-wall and cold-flow tests at the same stagnation pressure. This indicates that wall cooling is also important in the shock-wave boundary-layer interaction resulting in flow

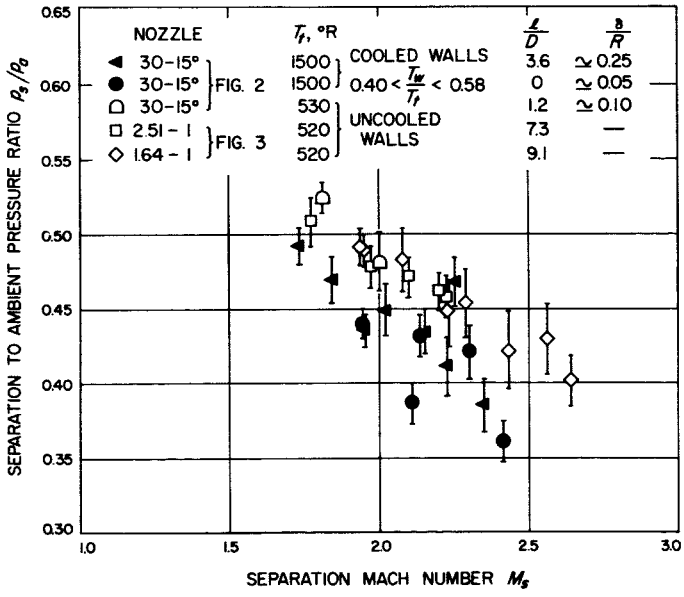

Fig. 7. Separation to ambient-pressure ratios for various nozzles

separation from the nozzle wall. Ahlberg et al. (Ref. 16) also found the same trend. For our data, it is not clear whether the lower separation pressures are due only to wall cooling, since, with hot flow and cooled walls, the boundary-layer-thickness Reynolds numbers at the separation point estimated from the analysis of Ref. 8 were about one half of those for cold flow at the same stagnation pressure and nozzle-inlet boundary-layer thickness. In this regard, the data shown in Fig. 7 for the 30–15-deg nozzle with hot flow and cooled walls do not reveal any definite trend between the results with relatively thin boundary layers ($\delta/R \simeq 0.05$) at the nozzle inlet and those with thicker layers ($\delta/R \simeq 0.25$). However, it is difficult to determine whether there is any boundary-layer-thickness Reynolds number dependence due to the scatter of the results at the highest separation Mach numbers (last four shaded points) which correspond to separation near the nozzle-exit plane.

The data in Fig. 7 extend over rather low stagnation-to-ambient pressure ratios because of the relatively small expansion-area ratios. When these data are compared to others obtained with uncooled walls, such as the accumulated results of Arens and Spiegler (Ref. 17, Fig. 2), the hot-flow cooled-wall data are found to lie below those results.

VII. MASS FLOW RATE

The large deviations from one-dimensional flow, particularly in the throat region, shown in Figs. 2, 3, and 4, direct attention to differences in mass flow rate that might be expected from one-dimensional flow predictions. In Fig. 8, comparisons between measured mass flow rate at a stagnation temperature of 1500°R (cooled walls) and computed values for one-dimensional isentropic flow ($\gamma = 1.35$) are shown in terms of the flow coefficient $c_d = \dot{m}/\dot{m}_1$. At the lower stagnation pressures, there is appreciable scatter in the values. Some of the scatter is undoubtedly due to errors in the mass flow rate measurements. At the higher stagnation pressures, the scatter is less, and for both nozzles, the flow coefficient is approximately between 0.98 and 1.0. Figure 8 also contains the inviscid flow prediction of Hall:

$$c_d = \frac{\dot{m}}{\dot{m}_1} = 1 - (\gamma + 1)\left(\frac{r_{th}}{r_c}\right)^2 \left[96 - \frac{8\gamma + 21}{4608}\left(\frac{r_{th}}{r_c}\right) + \frac{754\gamma^2 + 1971\gamma + 2007}{552960}\left(\frac{r_{th}}{r_c}\right)^2 - \cdots\right] \quad (4)$$

For the 30–15-deg nozzle, the prediction from Eq. (4) is 0.9943, in fair agreement with the experimental values. This correspondence is expected from the close agreement of predicted and measured static pressures in the throat region. However, for the 45–15-deg nozzle, the experimental values exceed the prediction from Eq. (4), in

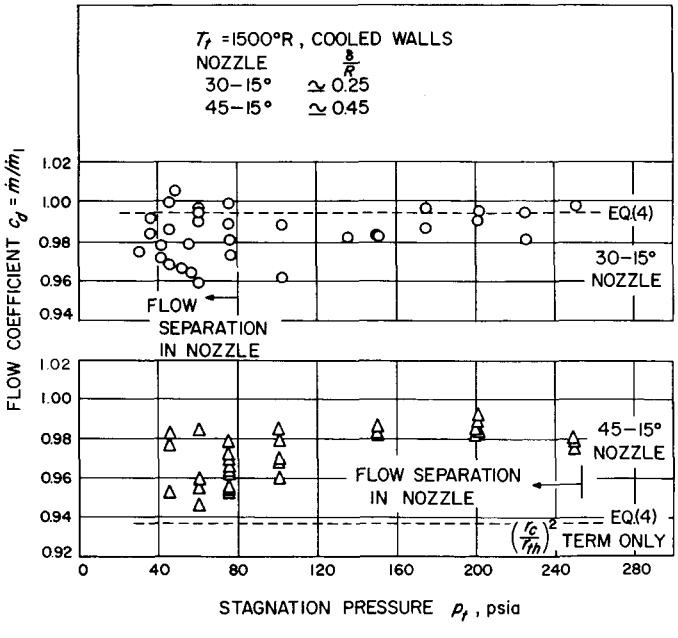

Fig. 8. Flow coefficients

which only the first term in the brackets is retained. As mentioned before, the Hall solution diverges for $r_c/r_{th} < 1$. If only the first term in the brackets is included, the prediction is identical to that of either Sauer (Ref. 10) or Oswatitsch and Rothstein (Ref. 13). Thus, the lower predicted values of the flow coefficient further show the inadequacy of existing predictions for nozzles with $r_c/r_{th} < 1$.

VIII. THRUST RATIOS

To indicate how the nozzles tested would perform as thrust devices, Fig. 9 shows ratios of actual thrust to that for one-dimensional isentropic flow ($\gamma = 1.40$) for a stagnation temperature of 1500°R (cooled walls):

$$\frac{F}{F_1} = \frac{(pA)_i + \int_{A_i}^{A} p\,dA}{(p_1A)_i + \int_{A_i}^{A} p_1\,dA} \tag{5}$$

To clearly illustrate the deviations, the nozzles are assumed to discharge into a vacuum, and the thrust ratios are shown for hypothetical expansion-area ratios from a value of 1 to that of the static-pressure tap location nearest the nozzle exit. The terms in the thrust expression represent the force on the nozzle-inlet area or effective chamber end wall and the integrated wall pressure distribution resulting in the axial force on the nozzle side wall. The shape of the thrust-ratio curve is dependent on whether the wall pressure is less or greater than the one-dimensional flow value and on the magnitude of the difference, as shown in Fig. 5. As the expansion-area ratio increases to about 1.5, the thrust ratio decreases as a result of the lower measured than one-dimensional flow pressures in this region. The thrust ratio then increases as the measured pressures exceed the one-dimensional values in the conical section. As was noted for the 45–15-deg nozzle, at larger expansion-area ratios,

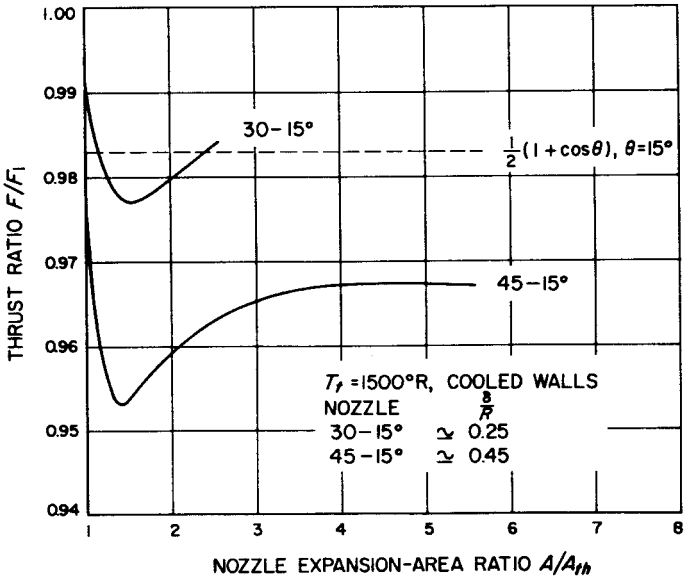

Fig. 9. Variation of thrust ratio with expansion-area ratio (Curves were obtained from averaged p/p_1 ratios shown in Fig. 5.)

the measured pressures again cross over and become less than the one-dimensional flow values. This leads to a slight decrease again in the thrust ratio. Shown for comparison is the often quoted correction factor, $\frac{1}{2}(1 + \cos\theta)$, for nonaxial exit flow for conical nozzles. Thrust ratios for cold flow would be the same as those shown in Fig. 9, based on the data in Fig. 2B.

IX. SONIC LINE

Table 1 contains a comparison at a stagnation temperature of 1500°R (cooled walls) of predicted and experimental location of the intersection of the sonic line with the edge of the boundary layer. The experimental values correspond to the point at which the Mach number obtained from the measured static-pressure distributions for isentropic flow ($\gamma = 1.35$) was equal to unity. One prediction for isentropic flow is from either Sauer (Ref. 10) or Oswatitsch and Rothstein (Ref. 13):

$$\frac{\xi}{r_{th}} = \left(\frac{\gamma + 1}{2}\right)^{1/2} \left(\frac{r_{th}}{r_c}\right)^{1/2} \tag{6}$$

where ξ is the axial distance upstream of the geometric throat. The other isentropic flow prediction is from Hall's analysis (Ref. 9). For the 30–15-deg nozzle, the prediction from Eq. (6) gives a value larger than that measured for the upstream distance to the sonic line, with better agreement afforded by Hall's prediction. Hall's analysis is not applicable to the 45–15-deg nozzle, since $r_c/r_{th} < 1$; by using Eq. (6), the predicted distance is more than twice the experimentally deduced value. The cold-flow experimental values would be the same as those indicated in Table 1, based on the data in Fig. 2B.

Table 1. Comparison of predicted and experimental sonic line intersection with edge of boundary layer at T_t = 1500°R (cooled walls)

Nozzle	$\left(\frac{\xi}{r_{th}}\right)_{exp.}$	$\left(\frac{\xi}{r_{th}}\right)_{Eq.\ (6)}$	$\left(\frac{\xi}{r_{th}}\right)_{Hall}$
30–15-deg	0.15-0.16	0.19	0.16
45–15-deg	0.13-0.14	0.34	–

X. MASS FLUX RATIOS

For the calculation of boundary-layer flow and heat transfer to nozzle walls, the local mass flux $(\rho V)_e$ at the edge of the boundary layer is needed. By assuming isentropic flow ($\gamma = 1.4$), this local mass flux was calculated from the measured static-pressure distributions and is shown nondimensionalized by the one-dimensional isentropic flow value in Fig. 10. Through most of the nozzle, the local mass flux is less than the one-dimensional value,

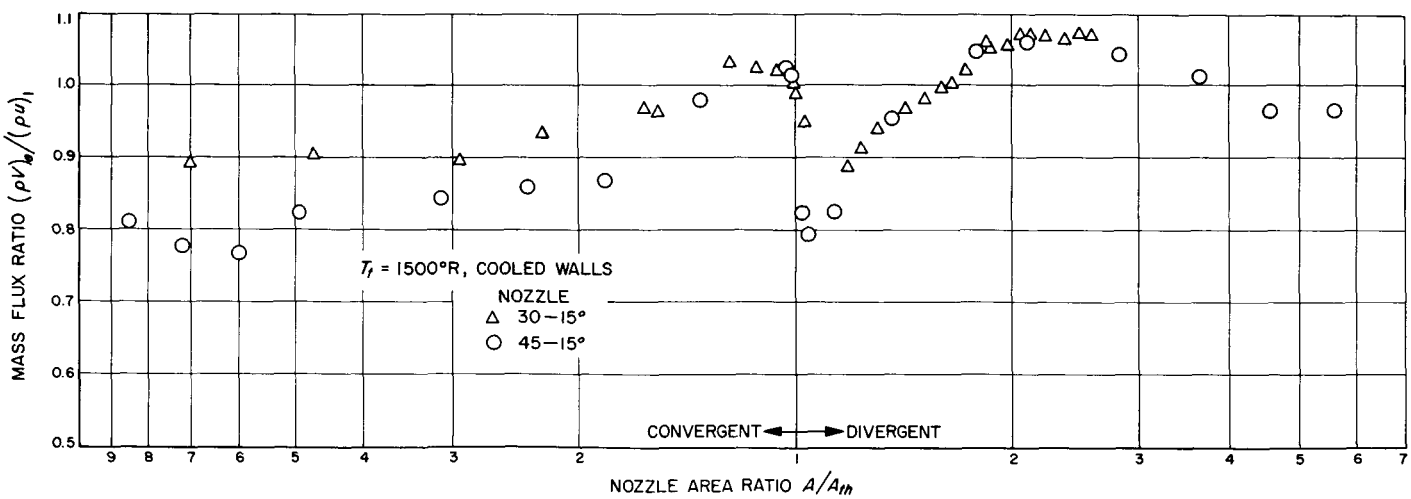

Fig. 10. Local to one-dimensional mass flux ratios along the nozzles (Values were determined from averaged p/p_1 ratios shown in Fig. 5.)

which implies lower wall heat fluxes, since for turbulent boundary-layer flows, $q \propto (\rho V)_e^{4/5}$. The slightly higher static pressures $p > p_1$ in the nozzle-inlet region observable in Fig. 5 result in larger differences in the mass fluxes. In this region, static pressures $p > p_1$ correspond to velocities $V < u_1$, since compressibility effects are unimportant. Conversely, in the supersonic region, the density decreases faster than the velocity increases so that the mass flux ratio is similar in trend to the pressure ratio p/p_1 in Fig. 5, but the deviations from one-dimensional flow are smaller in magnitude. The mass flux deviation amounts to about 20% in the inlet region and just downstream of the throat for the 45–15-deg nozzle; with the 30–15-deg nozzle, the deviations are less.

The maximum values of the mass flux $(\rho V)_e$ occur just upstream of the geometric throat at the intersection of the sonic line with the edge of the boundary layer. It is in this region that heat-transfer measurements indicate the maximum heat flux to the wall (Ref. 1, 6, 18).

XI. CONCLUSIONS

Wall static-pressure measurements have been presented for air flowing through circular-arc-throat conical nozzles. The results indicate the following:

1. In the throat region, the magnitude of the deviations in static pressure from one-dimensional flow depends on the ratio of throat radius of curvature to throat radius r_c/r_{th}. These deviations amount to as much as about 30 and 45% for the nozzles with $r_c/r_{th} = 2.0$ and 0.625, respectively, and are essentially independent of inlet configuration.

2. Smaller deviations in static pressure from one-dimensional flow were found in the conical sections. In the convergence region, the magnitude increases with convergence angle, while in the divergence region, this effect was not investigated since all the nozzles tested had a 15-deg half-angle of divergence.

3. For underexpanded operation, the pressure measurements were insensitive to the effects of both cooled and uncooled walls and to nozzle-inlet boundary-layer thickness to 0.45 of the nozzle-inlet radius. Thus, boundary-layer effects were found to be negligible.

4. Pressure readings depend on tap size, with differences up to 7% found between 0.010- and 0.040-in.-diameter holes. The smaller tap reads the lower pressure, which is believed to be nearer the true static pressure.

5. For overexpanded nozzle operation, the separation point moved downstream with wall cooling for tests at the same stagnation pressure, so that the hot-flow cooled-wall separation-to-ambient pressure ratios were generally about 5 to 10% below the cold-flow values.

6. Deviations in mass flow rate and thrust from predictions for one-dimensional flow appear to be due to the two-dimensionality of the flow, with boundary-layer displacement effects relatively unimportant for the nozzles investigated which have expansion-area ratios to 6.6.

7. In the throat region, local mass fluxes at the edge of the boundary layer deduced from the static-pressure measurements deviate less from one-dimensional flow values than do the static pressures. In the convergence section, the magnitudes of these deviations are about the same as they are in the throat region and depend on the convergence angle.

Two-dimensional flow predictions are in close agreement in the throat region with the data for the nozzles with $r_c/r_{th} = 2.0$ but inadequate for the nozzle with $r_c/r_{th} = 0.625$.

NOMENCLATURE

a speed of sound

a^* speed of sound at the sonic condition

A local nozzle cross-sectional area

A_{th} nozzle-throat area

c_d flow coefficient

d static-pressure tap diameter

D nozzle-inlet diameter

F axial thrust

l nozzle approach length

$\dot{m}$ mass flow rate

M Mach number

p wall static pressure

p_a ambient pressure

p_s separation pressure

p_t stagnation pressure

r nozzle radius

r_{th} nozzle-throat radius

r_c nozzle-throat radius of curvature

r_i nozzle-inlet radius of curvature

R nozzle-inlet radius

T_t stagnation temperature

T_w wall temperature

z axial distance from nozzle inlet

u velocity component in z-direction

V flow velocity at wall

γ specific-heat ratio

δ velocity boundary-layer thickness at nozzle inlet

δ^* displacement thickness

ε_c nozzle contraction-area ratio

ε_E nozzle expansion-area ratio

ν kinematic viscosity

ξ distance defined in Eq. (6)

ρ density

τ wall shear stress

Subscripts

e condition at free-stream edge of boundary layer

i condition at nozzle inlet

s condition at flow separation

t stagnation condition

1 one-dimensional flow value

REFERENCES

1. Back, L. H., Massier, P. F., Gier, H. L., "Convective Heat Transfer in a Convergent-Divergent Nozzle," *Int. J. Heat Mass Transfer*, Vol. 7, No. 5, pp. 549–568 (1964).

2. Scheller, K., Bierlein, J. A., "Some Experiments on Flow Separation in Rocket Nozzles," *ARS J.*, Vol. 23, No. 1, pp. 28–32, 40 (1953).

3. Frazer, R. P., Eisenklam, P., Wilkie, D., "Investigation of Supersonic Flow Separation in Nozzles," *J. Mech. Eng. Sci.*, Vol. 1, No. 3, pp. 267–279 (1959).

4. Campbell, C. E., Farley, J. M., *Performance of Several Conical Convergent–Divergent Rocket-Type Exhaust Nozzles*, NASA TN D-467, Sept. 1960.

REFERENCES (Cont'd)

5. Arens, M., Spiegler, E., "Separated Flow in Overexpanded Nozzles at Low Pressure Ratios," *Bull. Research Council of Israel*, 11C, No. 1, pp. 45–55 (1962).

6. Fortini, A., Ehlers, R. C., *Comparison of Experimental to Predicted Heat Transfer in a Bell-Shaped Nozzle with Upstream Flow Disturbances*, NASA TN D-1743, Aug. 1963.

7. Stanton, T. E., "The Variation of Velocity in the Neighborhood of the Throat of a Constriction in a Wind Channel," *British ARC Reports and Memoranda*, No. 1388 (1930).

8. Elliott, D. G., Bartz, D. R., Silver, S., *Calculation of Turbulent Boundary-Layer Growth and Heat Transfer in Axi-Symmetric Nozzles*, Technical Report No. 32-387, Jet Propulsion Laboratory, Pasadena, Feb. 15, 1963.

9. Hall, I. M., "Transonic Flow in Two-Dimensional and Axially-Symmetric Nozzles," *Quart. J. Mechanical and Applied Math.*, Vol. XV, Pt. 4, pp. 487–508 (1962).

10. Sauer, R., *General Characteristics of the Flow Through Nozzles at Near Critical Speeds*, NACA TM-1147, June 1947.

11. Darwell, H. M., Badham, H., "Shock Formation in Conical Nozzles," *AIAA J.*, Vol. 1, No. 8, pp. 1932–1934 (1963).

12. Migdal, D., Landis, F., "Characteristics of Conical Supersonic Nozzles," *ARS J.*, Vol. 32, No. 12, pp. 1898–1901 (1962).

13. Oswatitsch, K., Rothstein, W., *Flow Pattern in a Converging–Diverging Nozzle*, NACA TM-1215, March 1949.

14. Jaivin, G. I., *Effect of Hole Size on Pressure Measurements Made With a Flat-Plate Dynamic-Head Probe*, Technical Report No. 32-617, Jet Propulsion Laboratory, Pasadena, June 15, 1964.

15. Livesey, J. L., Jackson, J. D., Southern, C. J., "The Static Hole Error Problem," *Aircraft Engineering*, Vol. XXXIV, No. 396, pp. 43–47 (1962).

16. Ahlberg, J. H., Hamilton, S., Migdal, D., Nilson, E. N., "Truncated Perfect Nozzles in Optimum Nozzle Design," *ARS J.*, Vol. 31, No. 5, pp. 614–620 (1961).

17. Arens, M., Spiegler, E., "Shock-Induced Boundary Layer Separation in Overexpanded Conical Exhaust Nozzles," *AIAA J.*, Vol. 1, No. 3, pp. 578–581 (1963).

18. Kolozsi, J. J., *An Investigation of Heat Transfer through the Turbulent Boundary Layer in an Axially Symmetric, Convergent-Divergent Nozzle*, Aerodynamic Lab., Ohio State University, TM-8, July 1958.

JET PROPULSION LABORATORY *California Institute of Technology • 4800 Oak Grove Drive, Pasadena, California 91103*

October 27, 1965

Recipients of Jet Propulsion Laboratory
Technical Report No. 32-654

SUBJECT: Errata for Technical Report No. 32-654

Gentlemen:

It is requested that the following changes be made in your copy of Jet Propulsion Laboratory Technical Report No. 32-654 entitled, "Comparisons of Experimental with Predicted Wall Static-Pressure Distributions in Conical Supersonic Nozzles," by L. H. Back, P. F. Massier, and H. L. Gier, dated October 15, 1964:

1. On page 12, Eq. (4) should read

$$c_d = \frac{\dot{m}}{\dot{m}_1} = 1 - (\gamma + 1)\left(\frac{r_{th}}{r_c}\right)^2\left[\frac{1}{96} - \frac{8\gamma + 21}{4608}\left(\frac{r_{th}}{r_c}\right) + \frac{754\gamma^2 + 1971\gamma + 2007}{552960}\left(\frac{r_{th}}{r_c}\right)^2 - \cdots\right] \tag{4}$$

2. On page 14, Eq. (6) should read

$$\frac{\xi}{r_{th}} = \left(\frac{\gamma + 1}{32}\right)^{1/2}\left(\frac{r_{th}}{r_c}\right)^{1/2} \tag{6}$$

The values shown in Figure 8 (page 12) and Table 1 (page 14) were correctly derived from the above equations.

Very truly yours,

I. E. Newlan, Manager
Technical Information Section

IEN:bab

Telephone 354-4321 *Twx 213-449-2451*